Renewable Energy 244 (2025) 122634

Contents lists available at ScienceDirect

Renewable Energy

journal homepage: www.elsevier.com/locate/renene

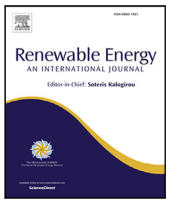

Application of hydrokinetic turbines in microtidal rivers: The Misa River test site

Matteo Postacchini [a],*, Gianluca Zitti [a], Eleonora Perugini [b,c], Riccardo Rossetti [a], Maurizio Brocchini [a]

[a] Department of Civil and Building Engineering, and Architecture (DICEA), Università Politecnica delle Marche, via Brecce Bianche 12, Ancona, 60131, AN, Italy
[b] Department of Civil & Environmental Engineering (CEE), University of Strathclyde, 75 Montrose Street, Glasgow, G1 1XJ, Scotland, UK
[c] Department of Civil Engineering, University of Birmingham, University Rd W, Building Y8,, Birmingham, B15 2FG, England, UK

ARTICLE INFO

Keywords:
Hydraulic modeling
Misa River
Microtidal environment
Hydrokinetic turbine
Archimedes screw turbine

ABSTRACT

The present study focuses on the potential application of Archimedes screw turbines in microtidal rivers. The Misa River, a 48-km long Italian course flowing into the Adriatic Sea, is taken as the reference test. Since hydrokinetic turbines operate with low discharges and require little engineering facilities, an Archimedes turbine was recently tested both in laboratory and numerically, showing performance coefficients up to 23.8%. To investigate its functioning within the Misa River, observed river stages are statistically analyzed and then used at the upstream boundary of a hydraulic model. The flow results are analyzed to evaluate the potential energy production of turbine configurations built upon a range of: (i) potential installation zones along the river, (ii) turbine radii, (iii) streamwise inclinations of the turbine axis. The energetic analysis of each configuration is performed accounting for one or more turbines installed along selected river cross-sections. A direct dependence is found between generated power and turbine size, especially for the inclined configurations. The optimal size and number of devices to be deployed at specific cross-sections are identified. The total annual energy for the best configurations is around 1 MWh, which may find application to supply energy to community buildings, like schools or kindergartens.

1. Introduction

One of the main challenges of the present century is the development of sustainable solutions in the field of energy production, through the use of renewable resources and new technologies. In such scenario, hydrokinetic turbines could play an important role, both for their low environmental impact and for their reduced costs, which make the design of hydrokinetic energy conversion systems an interesting research topic [1,2]. Some researchers highlighted the importance the micro-hydrokinetic turbines might have, in terms of economical, technical and environmental benefits, as they can operate in little or no water super-elevation [3]. Further, such turbines do not require significant and impacting infrastructures typical of hydropower plants, rather they have the advantage to be relatively flexible, e.g. quite easily accessed or retrieved in case of need/maintenance [4]. Therefore, these technologies provide a cost-effective source of electricity in rural areas, where distances are important, populations are small and energy demand is low [5,6].

Harnessing kinetic energy is a paradigm shift in extracting renewable energy from rivers. In the past, energy extraction from rivers was dominated by large hydropower plants, but the social and environmental impact of large infrastructures is pushing toward smaller and less impacting plants, like those using hydrokinetic turbines [7,8]. However, the application of such turbines in operational environments is still missing for several reasons. First, the relatively small efficiency of these turbines does not promote a significant investment in their development and optimization. On the other hand, there are many types of hydrokinetic turbines currently object of research and development, but the best solution on which focusing research and development activities has not yet been identified. This is also due to the different metrics by which these turbines are currently evaluated: not only energy performance, but also environmental and social impact.

In this context, different types of hydrokinetic turbines can be used in different configurations. Kirke [9,10] evaluated different candidate turbines for application in rivers, including multiple axial-flow turbines, various horizontal-axis Darrieus turbines, Archimedean screw types, water wheels, and belt turbines. The author highlights that the turbine type should be simple, potentially low cost, able to be built

* Corresponding author.
E-mail address: m.postacchini@staff.univpm.it (M. Postacchini).

https://doi.org/10.1016/j.renene.2025.122634
Received 8 May 2024; Received in revised form 23 January 2025; Accepted 5 February 2025
Available online 14 February 2025

in developing countries with limited workshop facilities, as well as suitably adjustable to improve their efficiency and power production. A common method to improve turbine performance and increase its efficiency (up to or above the Betz limit) is based on the exploitation of the blockage effect, achievable in different ways. Typical examples are based on either the reshaping of the river cross section (e.g., bed lifting) or the confinement of the turbine using a specific structure (e.g., a duct) [11–13].

Classical hydrokinetic screw turbines have been studied for long via both numerical modeling and laboratory experiments, and are characterized by a main body that is both emerged and submerged [14–16]. On the other side, ductless Archimedes turbines have recently been investigated, and are characterized by a completely submerged body, possibly inclined to the streamwise direction [17].

Different from the classical screw turbines, the ductless turbines are arranged in the fluid flow without any supply or protection system, in order to improve the benefits of the traditional hydrokinetic turbines. Notwithstanding its simplicity and the little requirements/infrastructures for its deployment, such device is still little considered for possible applications worldwide [18–21].

Hence, a potential field application is here hypothesized, based on the existing physical and numerical modeling recently undertaken for the complete characterization of the efficiency of such ductless Archimedean turbine [22], which is highly versatile and can be installed in several different configurations.

In detail, the present work aims at developing a hydraulic model of the Misa River (MR hereafter), taken to be representative of all microtidal rivers debouching into the Adriatic Sea and of small microtidal rivers in general, using the HEC-RAS software [23]. The MR is a water course located in the Central Italy, which flows for 48 km from the Apennine Mountains to the Adriatic Sea. The main forcing actions affecting the final stretch of the MR are of both riverine and marine nature. Specifically, the river current characterizes the whole river length, while sea/swell waves mainly affect the area nearby the mouth, especially during sea storms (upriver distance from the mouth of order $O(10\ \mathrm{m})$), and infragravity waves penetrate a bit further (upriver distances of order $O(100–1000\ \mathrm{m})$). However, although the microtidal environment (tidal range of about 40–50 cm), tides succeed in traveling upriver for long distances, i.e. with $O(10,000\ \mathrm{m})$ [24].

After the model calibration and following validation, the mechanical power and total energy of a series of hydrokinetic Archimedes screw turbines, potentially installed along the MR, are evaluated. Different turbine characteristics (number, size, inclination) and different river locations are used to compare several potential configurations.

The manuscript is organized as follows. Section 2 depicts the used material and methods. Section 3 illustrates and discusses the main findings. Finally, some conclusions close the paper.

2. Materials and methods

In the Central part of Italy, the Apennine Mountains give rise to the MR (Fig. 1a), whose watershed is approximately $383\ \mathrm{km}^2$ and its length about 48 km (more details in [25]). As most of the rivers of the Marche Region, the MR has a torrential regime, with weak flows during dry periods and very high flows (order of hundreds of cubic meters per second) during rainy periods. The watershed has narrow deep valleys in the upstream section and enlargements moving downstream, with the presence also of alluvial terraces. In the most downstream area, the MR crosses the town of Senigallia and then flows into a salt-wedge micro-tidal estuary, characterized by little river sea water exchanges. Notwithstanding the reduced tide range and the small flow exchange at the estuary, it has been demonstrated that the sea entrance provides significant effects in the lower reach of the MR [25].

The hydraulic model of the MR is built for a stretch long about 12 km, extending from the hydrometric station of Bettolelle to the MR mouth and characterized by no tributaries in between [26] (Fig. 1b).

Table 1
Investigated years with percentages of missing data. Years characterized by missing data over 70% are in boldface.

Year	Missing data	
	counts	%
2003	**17,520**	**100.00**
2004	**17,521**	**99.73**
2005	2,300	13.13
2006	3,908	22.31
2007	7	0.04
2008	17,731	10.09
2009	1,934	11.04
2010	860	4.91
2011	**13,962**	**79.69**
2012	9,051	51.52
2013	3,830	21.86
2014	829	4.73
2015	**12,861**	**73.41**
2016	**12,339**	**70.24**
2017	3,744	21.37
2018	0	0.00
2019	827	4.72
2020	7,623	43.39

Specifically, the upstream boundary condition is provided by the "Sistema Informativo Regionale Meteo-Idrio-Pluviometrico", managed by the "Centro Funzionale Multirischi" of the Regional Civil Protection. Hence, based on the water-surface level measured at Bettolelle, the typical year is first identified (Section 2.1). Furthermore, the model setup is described in terms of geometry, boundary conditions, calibration and validation (Section 2.2). The laboratory and numerical findings concerning the hydrokinetic turbines and used in the present work are then summarized, with the aim to illustrate the baseline for the calculation of both mechanical power and energy production (Section 2.3).

2.1. The typical year

The water-surface levels at Bettolelle, used for the analysis of the typical year, cover the time range from 2003 to 2020. We here use the stage data defined as "validated", which only includes suitable recordings, with unreliable recording caused by sensor damages, obstructions, etc. being removed.

Table 1 shows the percentage of missing data, which is relevant for the following analysis, as only years with missing data percentages smaller than 70% are considered.

The rating curves, provided by the Regional Civil Protection website, are used to estimate the flow discharge at each time, in order to evaluate the daily averages.

Based on the daily average discharges, the duration curve of each year is obtained. Further, the average duration curve is calculated by averaging the duration curves of the single years. All single-year duration curves (colored lines) and the average duration curve (black dotted line) are shown in Fig. 2, where years characterized by more than 70% of missing data are not illustrated.

With reference to the curves illustrated in Fig. 2, Table 2 shows both the percentage of missing data for each considered year (second column) and the standard deviation (STD hereafter) of each curve with respect to the average duration curve (third column).

Although the resulting STD suggests that 2012 is the year which is the closest to the average one, its missing data are over 50% and we assume not to take it into account, due to the extremely scattered time series. For such reason, the 2018 is selected as the typical year for the following hydraulic modeling. Being thus the typical year chosen, the data of the hydrometric station located at Ponte Garibaldi (Fig. 1b) and related to 2018 are used for the model calibration (from 18 February to 07 March 2018) and validation (whole 2018).

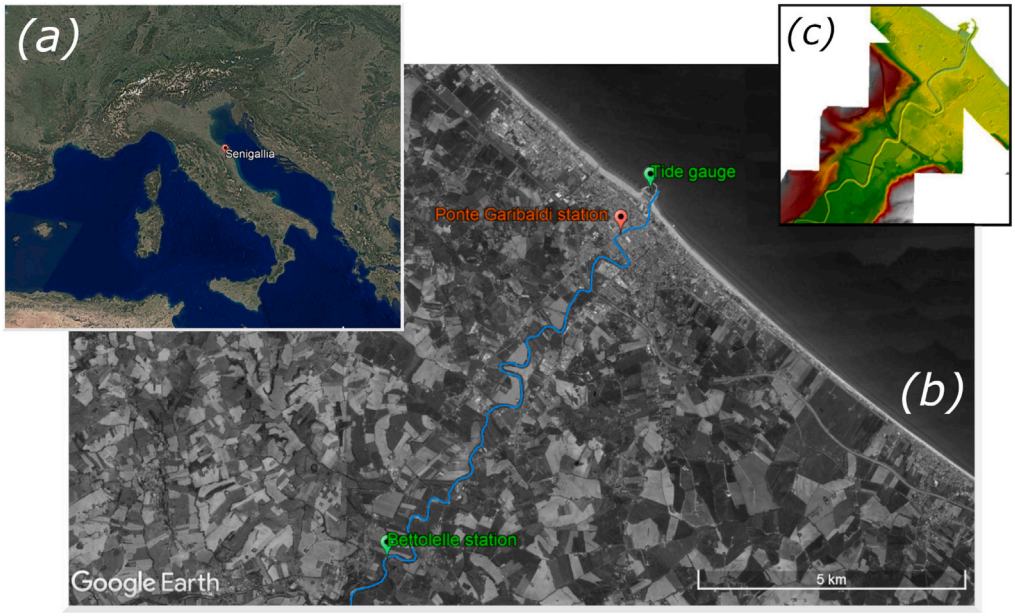

Fig. 1. Study site. **(a)** Italy map. **(b)** Stretch of the Misa River (in blue) and location of stations used for the hydraulic modeling. **(c)** DTM employed for the setup of the modeled terrain.

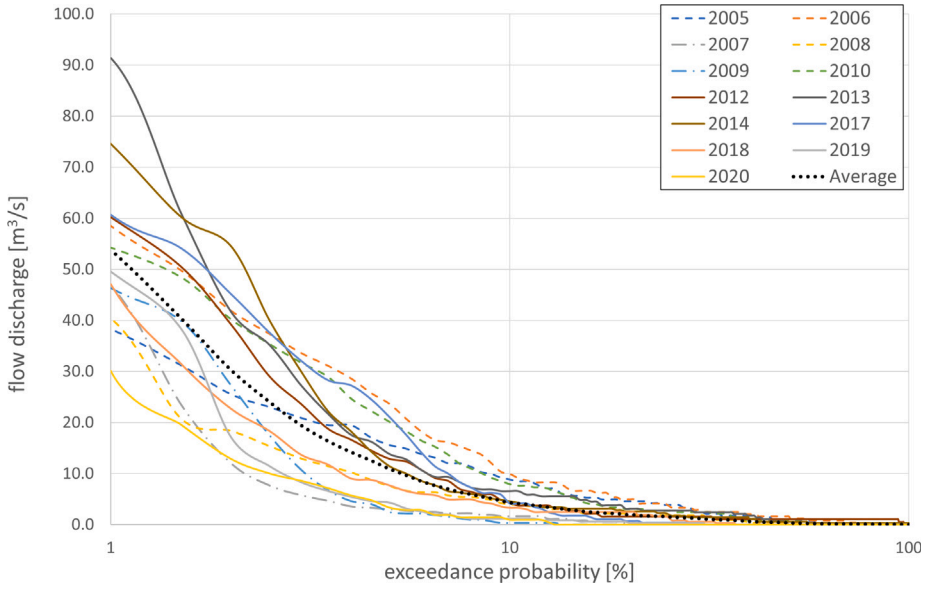

Fig. 2. Duration curves of flow discharge at Bettolelle between 2005 and 2020 (semi-logarithmic trend). The average year is represented by a black dotted line.

2.2. The model setup

The model implementation is carried out using the 1D Unsteady Flow solver of the HEC-RAS software, developed by the US Army Corps of Engineers in 1995 at the Hydrologic Engineering Centre (HEC) in Davis, California [23]. The numerical model is based on a recently developed baseline project [26], and the first aim of the present work is to improve such model by adjusting the input parameters and reach a reliable flow propagation in the final stretch of the MR. Such procedure has been characterized by several enhancements and the following parameters have been adjusted passing from the baseline project to the final improved model:

- Geometric/terrain data, i.e. DTM terrain files, cross-section geometry, bathymetry at the estuary.
- Upstream boundary condition, i.e. hydrograph at Bettolelle cross-section.
- Downstream boundary condition, i.e. tidal stage at the river mouth.

In the baseline project, the main topographic data refer to a 2008 survey carried out by the "Ministero dell'Ambiente e della Tutela del Territorio e del Mare" (Fig. 1c), and have been used to define a number of cross-sections along the investigated river stretch [26]. Later on, some cross-sections have been implemented or updated using the 2019 data either provided by the Regional Civil Protection (area of Bettolelle) or surveyed by our team during a recently concluded project (area of Ponte Garibaldi). A further bathymetry has also been used in the final 600 m of the MR, being this surveyed during the typical year, i.e. in 2018. The river stage at all control sections has been referred to the mean sea level.

Concerning the boundary conditions, the following inputs have been used: a flow hydrograph (and then a stage hydrograph) at the

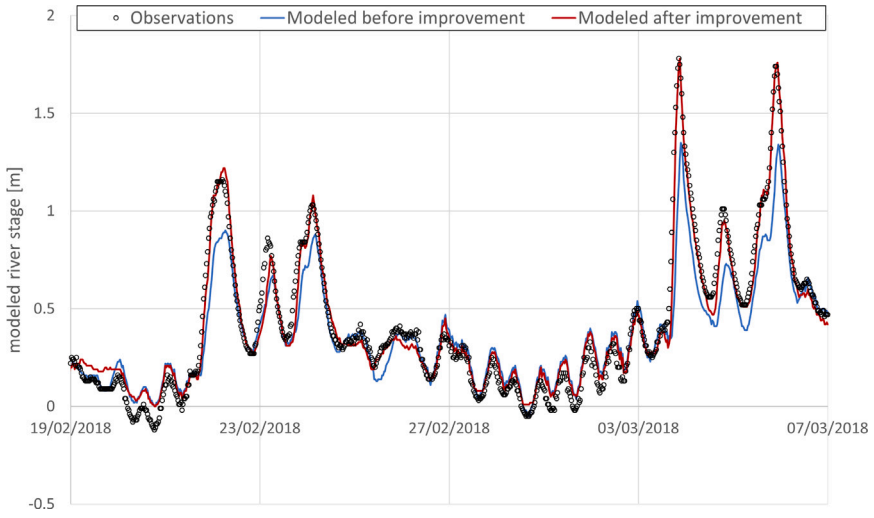

Fig. 3. Time-series comparison at Ponte Garibaldi from 18 February to 07 March 2018 (calibration): stage observations (black dots) and numerical results for the baseline project (blue line) and after the improvements (red line).

Table 2
Selected years with missing data less than 70% and STD referring to the curves shown in Fig. 2.

Year	Missing data [%]	STD
2005	13.13	2.92
2006	22.31	3.63
2007	0.04	3.13
2008	10.09	2.67
2009	11.04	2.47
2010	4.91	2.80
2012	51.52	1.41
2013	21.86	3.92
2014	4.73	3.44
2017	21.37	2.83
2018	0.00	1.98
2019	4.72	2.44
2020	43.39	3.65

upstream section.[1] and the sea level from Ancona tide gauge at the downstream section[2] Such sea level recordings well agree with the sea levels measured at Senigallia, where the local tide gauge started recording only in July 2018 [27]. Although the sea actions entering the MR mouth and leading to complex 3d river-sea interactions, typical of estuarine zones [25,28], recent works testify the suitability of using stage hydrograph coming from tidal stages at the downstream boundary [29].

Starting from such baseline project, a calibration process has been undertaken using the data collected in the period between 18 February and 07 March 2018. To this aim, observed and modeled stage values have been compared at a control station, i.e. Ponte Garibaldi (red pin in Fig. 1b), evaluating the root mean square error (RMSE) between the HEC-RAS/modeled results and the data collected by the Regional Civil Protection.

The comparison between collected data (black circles in Fig. 3) and modeled results at Ponte Garibaldi shows that the baseline hydraulic model (blue line) cannot properly catch the river stage, especially during flood conditions. Such behavior is well represented by the scatter plot of Fig. 4, where many of the blue dots are below the black bisector, indicating an underestimate of the river stage. However, the above-described model improvements and the optimization of the Manning coefficients along the MR has led to a significantly improved result, as shown in red within such figures. In particular, Fig. 4 illustrates the interpolating colored lines and the statistics related to such interpolations. The effective model improvement is testified by the reduced dot dispersion around the bisector, as well as by a strong decrease of the RMSE, which changes from 0.15 m to 0.06 m.

Subsequently, the model has been validated over the whole 2018, i.e. the typical year, as shown in Fig. 5. The simulation provides good results for the wet periods (e.g., flood peaks), though some discrepancies in the middle part of the graph, which refer to dry periods. This is probably due to the fact that the present hydraulic model does not take into account infiltration/exfiltration processes, i.e. the flux exchanges between surface-water and groundwater flows. In particular, the water table is lower in summer, when the water infiltrates from the river (losing-river condition) and causes a river-stage lowering. On the other hand, such flux is lower or negative in autumn and winter, when the water table is higher (gaining-river condition).

Additional comparisons between modeled and observed data, at different locations and times, are discussed in [30] and provide fairly good results. Specifically, some observations carried out in January 2014 in the lower reach of the MR [24] are compared with the modeled results obtained using the HEC-RAS software. The comparisons referring to two tide gauges located about 280 m (TGdown) and 580 m (TGup) from the MR mouth, are illustrated in Fig. 6. These show a fairly good agreement in terms of low-frequency components (i.e., tide, storm surge), while the higher frequency components (i.e. wind and swell waves propagating upriver during stormy and quiescent conditions) are not captured, as the downstream boundary condition of the model is based on the low-frequency oscillations recorded at the Ancona harbor.

2.3. The archimedean turbine

A ductless Archimedes screw turbine, recently studied both numerically and via laboratory tests [17,22], has been chosen for a possible application in the present site. In fact, such turbine type: is simple and cheap, therefore it can be used in locations with limitations, such as in shipping areas; reduces environmental impacts; does not require the construction of civil infrastructures (barrages, reservoirs); works also in small water depths; maximizes the flow energy exploitation. An image and a sketch of the geometry of the turbine are reported in Fig. 7.

The design of the turbine for the laboratory tests was inspired by Archimedean screws used in small hydropower plants. According to

[1] Regional Civil Protection website: http://app.protezionecivile.marche.it/sol/

[2] ISPRA website: https://www.mareografico.it/

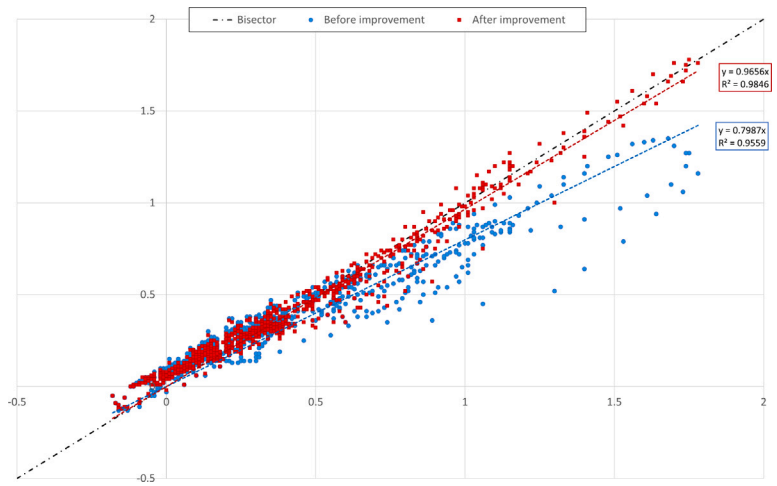

Fig. 4. Scatter-plot comparison at Ponte Garibaldi from 18 February to 07 March 2018 (model calibration): stage observations VS numerical results for the baseline project (blue) and after the improvements (red).

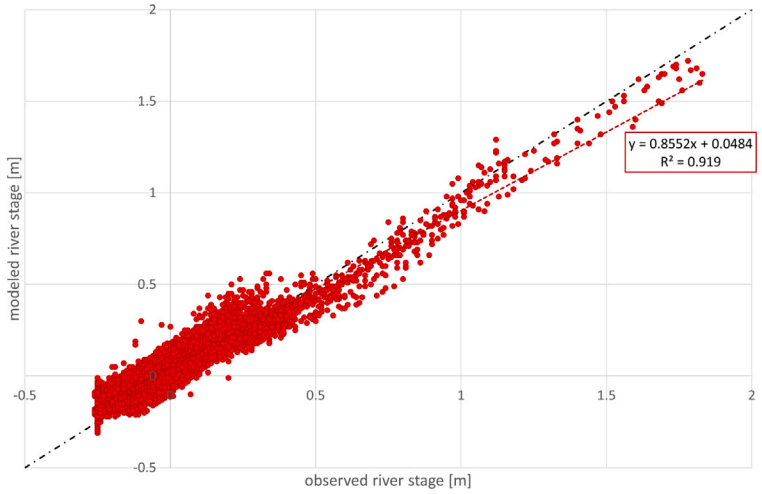

Fig. 5. Scatter-plot comparison at Ponte Garibaldi during the whole 2018 (model validation): stage observations VS modeled results.

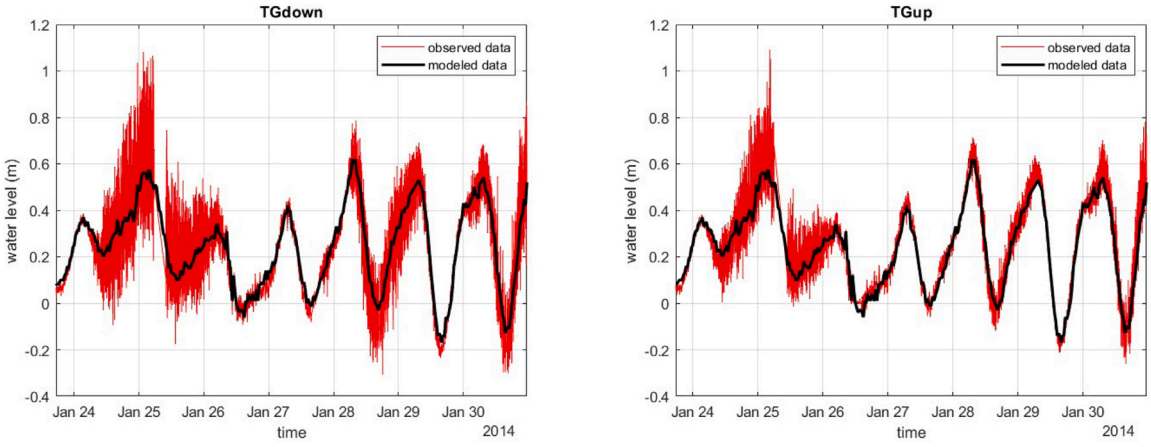

Fig. 6. Comparison between modeled results (black) and field observations (red) at about 280 m (TGdown, left panel) and 580 m (TGup, right panel) from the MR mouth.

the size of the flume that was used for the experimental tests, the turbine was designed with a radius equal to 0.1 m and two blade strides. A tubular aluminum axle, with diameter of 12 mm and thickness of 1 mm, providing stiffness and resistance to the turbine. The screw was manufactured in polylactic acid (PLA) using a 3D printer, resulting in 5 mm thick blades, 160 mm long-stride, and a blade inclination with respect to the turbine axis of 70°.

As all the hydrokinetic turbines, the efficiency of the Archimedes turbine is evaluated on the basis of the Betz' theory [31], using the performance coefficient C_p, which allows for an estimate of the mechanical

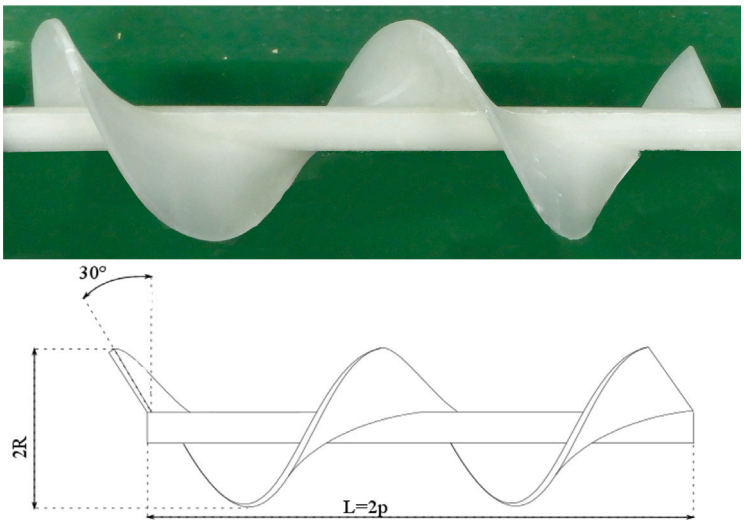

Fig. 7. Image (top panel) and sketch with the main characteristics (bottom panel) of the screw turbine investigated in Zitti et al. [22].

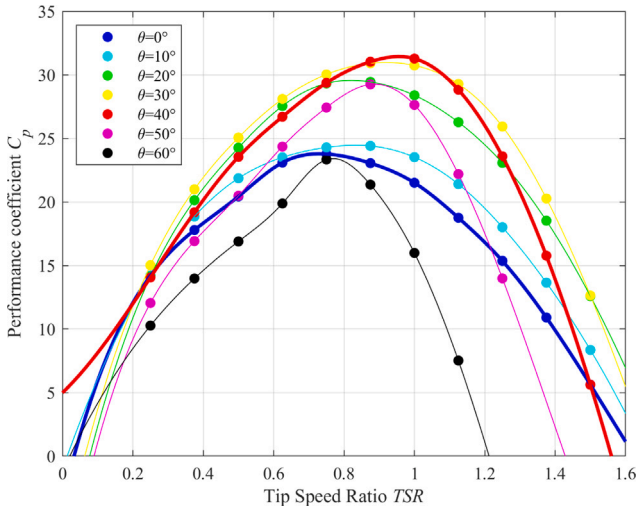

Fig. 8. Performance curves of the Archimides screw turbine proposed by [22], for different inclination of the turbine axis with the stream direction θ.
Source: Bullets are taken from the numerical results of [17]

power P_e that can be captured by the turbine:

$$P_e = C_p P_a \tag{1}$$

where P_a is the available power from the river flow, given by:

$$P_a = \frac{1}{2} A_t \rho V^3 \tag{2}$$

where A_t is the cross-flow sectional area of the turbine, ρ is the fluid density and V is the section-averaged stream flow velocity. The efficiency at different inclinations with respect to the stream direction θ and different tip speed ratios ($TSR = \omega R/V$, being ω the rotational speed of the turbine) was estimated by Zitti et al. [17]. Being R the turbine radius and evaluating the cross-flow sectional area of the turbine as $A_t = R^2\pi$ regardless of its inclination θ, the performance curves were extracted and are reported in Fig. 8.

The best performances is provided by the configuration with the turbine axis is inclined to the stream direction of $\theta = 40°$, which shows $C_p \leq 30\%$ for $TSR \in (0.875, 1)$ (red line). On the other hand, the flow-aligned configuration ($\theta = 0°$, blue line) actually exploits the lowest size of cross-flow sectional area and still provides good performances, being $C_p \leq 20\%$ for $TSR \in (0.5, 1)$. These two cases are considered for the evaluation of the extracted power using Eqs. (1) and (2).

3. Results and discussion

The hydrodynamics along the MR obtained for the 2018 simulation have been used for the analysis of the potential mechanical power and energy production assessment. Specifically, Section 3.1 investigates both average flow velocity and water surface at each modeled cross-section, in order to find a suitable location for the installation of a hydrokinetic turbine system. Different possible configurations are discussed in Section 3.2 and the power estimate and the annual energy assessment are discussed in Section 3.3.

3.1. Overall hydrodynamics and turbine location

To properly choose the best cross-sections where to potentially locate the turbines, the hydrodynamic results coming from the 2018 simulation (see Section 2.2) are used. An example of the modeled results is shown in Fig. 9, which depicts both the instantaneous water depth (panel a) and averaged velocity (panel b) occurring on 24 February 2018 at 3:00.

The potential locations have been selected, mainly on the basis of: easy and convenient installation (e.g. close to existing structures); flow-velocity increase (e.g. due to channel narrowing), which provides an improvement of the available power. According to such criteria, some cross-sections have been selected nearby the following bridges (see arrows in Fig. 10):

- Ponte Portone (1.84 km upstream of the MR mouth)
- Ponte A14 (3.22 km upstream of the MR mouth)
- Ponte Borgo Catena (4.03 km upstream of the MR mouth)
- Ponte Cannella-Vallone (7.87 km upstream of the MR mouth)

Further cross-sections have been selected on the basis of the high velocity found at their location, i.e. 3.39 km, 4.66 km, 5.33 km and 6.40 km far from the MR mouth (see circles in Fig. 10). A list of the considered cross-sections is reported in Table 3.

The procedure below described has been followed to define suitable turbine configurations at each location.

– The duration curves of the water surface elevation have been built at each cross-section, and a maximum reference radius R_{max} has been calculated as the maximum value obtained by subtracting the riverbed level from the water-surface elevation with 90% exceedance probability ($WS_{90\%}$), reduced of 0.2 m (Table 3). Such reduction is based on the necessity of avoiding

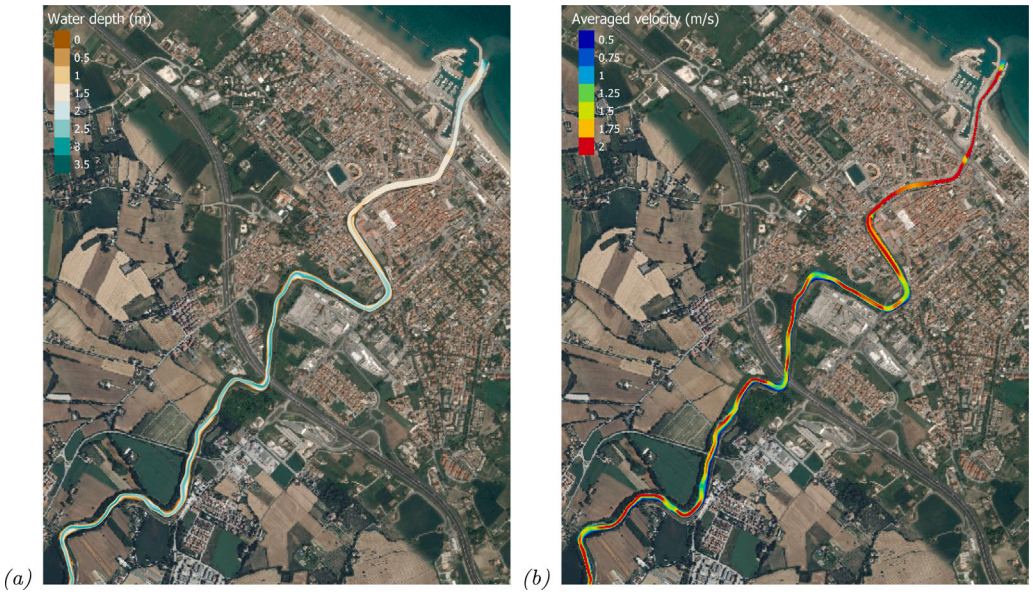

Fig. 9. *(a)* Water depth and (*b*) section-averaged velocity on 24 February 2018 at 3:00.

Fig. 10. Portion of the studied MR stretch, with indication of the selected cross-sections: bridges (yellow arrows and labels) and high flow areas (yellow circles).

or reducing sediment-transport issues, i.e. erosion/deposition patterns, promoted by the additional bottom friction generated by the turbines. For the energy assessment, which is the object of the present hydrodynamic study, it is assumed that the vertical location of the turbines is updated in time according to the morphological evolution of the riverbed.

– The cross-section-dependent activation level (AL) of each turbine is evaluated as the level over the riverbed that provides the complete submergence of the turbine, i.e. the sum between the turbine radius and the buffer value of 0.2 m. In this phase, considering the turbine radius equal to the maximum reference radius R_{max}, it follows that $AL = WS_{90\%}$.

– Finally, the available energy of the entire year is estimated at each river cross-section using the following relation:

$$E_{av} = \sum_i P_{a,i} \Delta t \tag{3}$$

where $P_{a,i}$ is the available power at time step i (see Eq. (2), where A_t is the total area of the river cross-section), while Δt is the time interval used in the simulation, i.e. 30 min.

The results for each selected cross-section, i.e. the maximum ideally exploitable energy by a single turbine, are reported in the last column of Table 3.

It can be observed that almost all the free-flow cross-sections are characterized by $R_{max} < 0.20$ m, hence suggesting one to work with a relatively little turbine size. The only free-flow section with $R_{max} > 0.20$ m is typified by an available energy comparable with that exerted

Table 3
Summary of main characteristics of the selected cross-sections.

Cross-section	Distance from mouth [km]	$WS_{90\%}$ [m]	R_{max} [m]	E_{av} [MWh]
Ponte Portone	1.84	0.80	0.30	24.41
Ponte A14	3.22	0.60	0.20	59.96
Free flow	3.39	0.59	0.19	47.89
Ponte Borgo Catena	4.03	0.78	0.29	84.93
Free flow	4.66	0.51	0.15	93.85
Free flow	5.33	0.51	0.15	121.22
Free flow	6.40	0.71	0.25	109.21
Ponte Cannella-Vallone	7.87	0.66	0.23	109.95

at Ponte Cannella-Vallone. Turbines with radius $R > R_{max}$ may be used, but such a choice would induce a higher activation threshold (AL) and a reduced operational time (see Section 3.2). Hence, due to the above reasons and to the good amount of available energy nearby bridges (e.g. compare the available energy at Ponte Cannella-Vallone with that available at the cross-section 6.4 km far from the mouth), as well as to the higher ease of installation, only the cross-sections close to bridges have been taken into account in the following.

3.2. Turbines configuration and operation

Considering the flow characteristics of the MR and the limitations given by the water elevation described in Section 3.1, specific turbine configurations are identified at the selected cross-sections and the annual energy production is evaluated for each of them.

In agreement with existing studies [32] and patents [33], a floating installation is considered. Specifically, the hydrokinetic turbines are supposed to be set on a floating support, which could be anchored to bridge piers and equipped with support legs. The floating system has been chosen for its ease of installation and maintenance, and keeps the turbine near the surface, where higher velocities are reached. The support legs are needed to keep the turbine always above the riverbed, at a minimum distance of 0.20 m, even when the support system is not floating, to avoid or reduce sediment-transport issues and turbulent fluctuations occurring within the bottom boundary layer.

However, although local erosion and sediment deposit may affect the flow around the turbine, bathymetric variations are not considered in the present study, this not preventing the turbine operation. Specifically, on the one side, the vertical location of each turbine follows the morphological evolution of the riverbed, according to its support legs. On the other side, the scour-deposition patterns generated by the turbine itself affect the energy assessment to a limited extent, as testified by recent works, where the TSR was even larger ($TSR \gg 1$) than that characterizing our scenarios ($TSR \sim 1$) [34–36].

Two turbine orientations are analyzed: one aligned along the streamwise direction ($\theta = 0°$), characterized by a maximum performance coefficient $C_p = 0.238$ achieved for $TSR = 0.75$; another inclined to the stream direction of $\theta = 40°$, which provides the best performance coefficient $C_p = 0.313$ when $TSR = 1$ (see Fig. 8). The use of the best C_p is supported by the exploitation of an electronic device to regulate the turbine rotational speed (ω) based on the water flow (V), in order to guarantee the optimal turbine performance. The sketches of the two possible floating systems, to be used for a single turbine installation, are reported in Fig. 11.

Consistently with the maximum reference radius evaluated in the previous section (see Table 3), three different radii have been considered: $R = 0.20$ m, 0.25 m and 0.30 m. Based on such radii, the activation level (AL) is calculated for each turbine in each configuration. As defined above, AL is the minimum free surface elevation providing the complete submersion of the turbine at its specific location. Hence, it is estimated as the riverbed level plus the turbine radius (either 0.20 m or 0.25 m or 0.30 m) plus the minimum distance from the riverbed (0.2 m). When the design turbine radius is larger than the maximum reference radius ($R > R_{max}$), the consequent AL is larger than $WS_{90\%}$, this indicating that the turbine will operate for a time shorter than 90% of the year. Although a partial submersion would even activate the turbine, leading to a limited power production, such occurrence is disregarded, as a conservative measure in the energy production assessment.

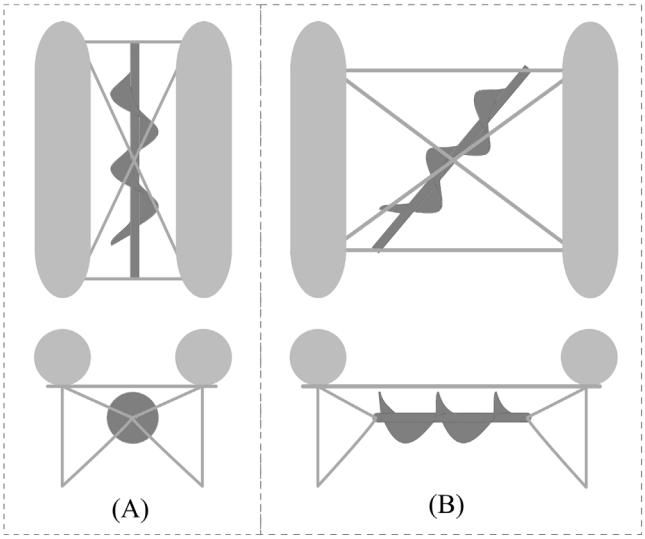

Fig. 11. Sketches of the floating support system for the single turbine: (A) flow-aligned ($\theta = 0°$) and (B) inclined ($\theta = 40°$) configurations with respect to the stream direction. Representation of top view (top panels) and cross-section view (bottom panels). Floating elements are in light gray.

Both flow-aligned and inclined configurations are considered for multiple installations in parallel within the considered cross-section. To satisfy the condition of undisturbed flux of Betz law, the axes of the flow-aligned turbines are located at least six radii apart within the cross-section plane. Such consideration leads to a precautionary estimate of the turbine performances, because the mutual and beneficial effects existing in multiple turbine installations are not accounted for, although these may potentially lead to an increase of the real C_p. However, specific numerical studies are currently underway to investigate such mutual effects, as well as the influence of the riverbed on the turbine operation.

In the inclined configuration, the spacing is evaluated accounting for the projected area of the turbines included in each river cross-section. Each different radius considered for the analysis leads to a different number of turbines that could be installed at each location.

As an example, Figs. 12 and 13 show the six different configurations potentially exploitable at Ponte Cannella-Vallone location (see Section 3.3). In detail, the minimum (WS_{min}) and maximum (WS_{max}) water levels occurring during the year are reported, together with $WS_{90\%}$ and the activation level related to each turbine (AL).

3.3. Power and energy evaluation

The power generated by each turbine is evaluated using Eq. (2) and the section-averaged velocity. Specifically, the velocity should be evaluated considering the classical logarithmic distribution, with the depth-averaged velocity corresponding to the velocity at a distance from the water surface of 60% of the whole depth. However, since the turbines are not deployed significantly close to the riverbed nor to the riverbanks, the local velocity, i.e. that affecting each turbine in correspondence of its axis, is quite similar to the cross-section-averaged velocity. This is thus used for the power calculation.

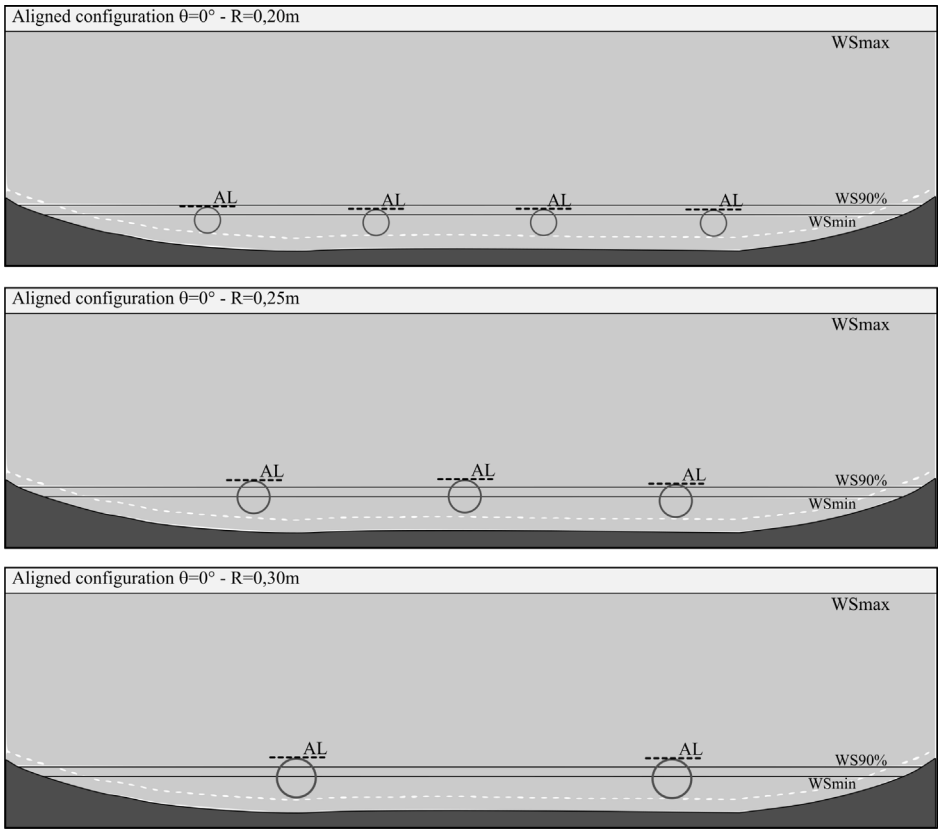

Fig. 12. Configurations with turbines aligned with the flow stream at Ponte Cannella-Vallone cross-section, including: the minimum (WS_{min}) and maximum (WS_{max}) water surface elevation in the reference year, the water-surface elevation with 90% exceedance probability ($WS_{90\%}$), the minimum distance of the turbine from the riverbed (white dashed line) and the activation threshold of each turbine (AL).

According to the turbine configurations analyzed in the previous sections, the energy harvested in 2018 is calculated at selected cross-sections. First, the power extracted from the kth turbine of each configuration at the ith time interval ($P_{e,k,i}$) is calculated using Eq. (1), while the energy harvested during the whole year using either the kth turbine (E_k) or the whole set of turbines of each specific configuration (E_{tot}) is, respectively, evaluated as:

$$E_k = \sum_i P_{e,k,i} \Delta t \tag{4}$$

$$E_{tot} = \sum_k E_k = \sum_k \sum_i P_{e,k,i} \Delta t \tag{5}$$

Table 4 illustrates the estimates related to the single turbines, as well as the total annual energy harvested for each configuration (E_{tot}) and the turbine-averaged harvested energy ($\overline{E}$). All energy values are given in kWh.

From the analysis of the annual energy production from the different configurations, the best results are obtained at the upstream cross-sections, where the flow velocity is larger and the cross-section shapes provide a natural duct/convergent for the flow towards the turbines. For a better understanding of the comparison in terms of turbine setting and location, Fig. 14 illustrates the annual energy production of the six different configurations tested at the four cross-sections. In general, the best results are not easily correlated with the inclination nor to the radius change, also considering that the increase of the radius reduces the number of turbines within the cross-section and increases the activation threshold (see Section 3.1).

Specifically, at Ponte Portone (blue bars), the best configurations are those characterized by $R = 30$ cm with $\theta = 0°$ and $R = 25$ cm with $\theta = 40°$, providing $E_{tot} \cong 205$ kWh. Differently, the best configurations at Ponte A14 (orange bars) are both related to $R = 20$ cm with either $\theta = 0°$ or $40°$, providing $E_{tot} \cong (270–280)$ kWh. Moving upstream, all tested configurations provide an annual energy $E_{tot} > 670$ kWh. The best solutions at Ponte Borgo Catena are those referring to $R = 25$ cm with $\theta = 0°$ and $R = 30$ cm with $\theta = 40°$ (gray bars), while the optimal configurations are associated with $R = 20$ cm with either $\theta = 0°$ or $\theta = 40°$ at Ponte Cannella-Vallone (yellow bars).

From the comparison among the configurations with a specific inclination (either $\theta = 0°$ or $40°$), rarely the energy production increases monotonically with the turbine radius. In particular, the energy production increases and then decreases with the radius in the flow-aligned configurations at Ponte Borgo Catena. This is caused by the simultaneous occurrence of the turbine-size increase (from $R = 20$ cm to $R = 30$ cm) and the reduction of the installed turbines (from 4 to 2), as shown in Table 4. In detail, the radius increase from 20 cm to 25 cm provides an increase of both cross-flow area A_t and, consequently, mechanical power and energy produced by the single kth turbine. Such energy increase can be represented by a coefficient $\frac{E_{k,25\ \mathrm{cm}}}{E_{k,20\ \mathrm{cm}}} \sim 1.56$ (see Eqs. (2) and (3)). Similarly, passing from $R = 25$ cm to $R = 30$ cm, the energy increase is represented by a coefficient $\frac{E_{k,30\ \mathrm{cm}}}{E_{k,25\ \mathrm{cm}}} \sim 1.2$. However, assuming that each turbine produces the same amount of energy, the reduction of the turbine number within the cross-section leads to a reduction of the harvested energy E_{tot}, which can be represented by a multiplying coefficient of 0.75 and 0.67, respectively passing from 4 to 3 turbines and from 3 to 2 turbines (see Eq. (5)). Accounting for both variations, passing from $R = 20$ cm to $R = 25$ cm provides an overall energy increase of ~17% (coefficient: $1.56 \cdot 0.75 = 1.17$), while passing from $R = 25$ cm to $R = 30$ cm leads to a decrease of ~20% (coefficient: $1.2 \cdot 0.67 = 0.80$).

Similarly, for the 40° configurations at Ponte Cannella-Vallone, the energy first decreases, because of the reduction of the installed turbines from 3 (for $R = 20$ cm) to 2 (for $R = 25$ cm), and then increases,

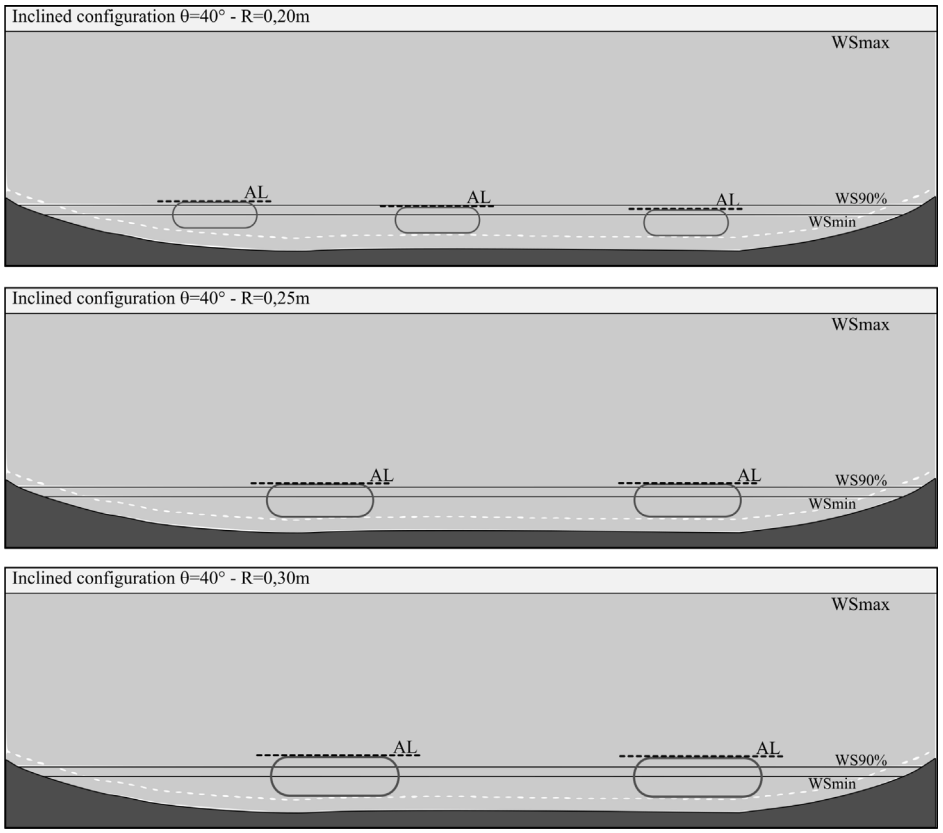

Fig. 13. Configurations with turbines inclined of $\theta = 40°$ with respect to the flow stream at Ponte Cannella-Vallone cross-section. The illustrated quantities are described in the caption of Fig. 12.

Table 4
Summary of the energy analysis referring to the whole 2018. The harvested energy is given in kWh.

Cross-sect.	Energy	Aligned ($\theta = 0°$)			Inclined ($\theta = 40°$)		
		$R = 20$ cm	$R = 25$ cm	$R = 30$ cm	$R = 20$ cm	$R = 25$ cm	$R = 30$ cm
Ponte Portone	E_1	15.83	27.52	29.95	18.87	28.14	45.29
	E_2	18.07	27.94	32.69	23.73	36.62	43.48
	E_3	18.12	27.85	37.98	23.73	36.82	43.48
	E_4	17.96	27.99	32.69	23.83	36.74	48.49
	E_5	18.12	28.10	39.63	23.83	37.09	–
	E_6	18.12	28.20	32.28	23.83	29.85	–
	E_7	18.12	27.52	–	23.83	–	–
	E_8	18.12	–	–	18.87	–	–
	E_9	18.12	–	–	–	–	–
	E_{10}	16.88	–	–	–	–	–
	E_{tot}	**177.48**	**195.12**	**205.21**	**180.53**	**205.26**	**180.74**
	$\overline{E}$	*17.75*	*27.87*	*34.20*	*22.57*	*34.21*	*45.19*
Ponte A14	E_1	63.06	98.53	100.89	71.34	116.28	129.35
	E_2	118.57	91.96	–	125.92	106.15	–
	E_3	86.66	–	–	80.01	–	–
	E_{tot}	**268.30**	**190.49**	**100.89**	**277.27**	**222.43**	**129.35**
	$\overline{E}$	*89.43*	*95.24*	*100.89*	*92.42*	*111.22*	*129.35*
Ponte Borgo Catena	E_1	191.61	307.29	412.91	251.99	407.30	494.26
	E_2	199.31	307.29	354.34	262.11	400.37	414.33
	E_3	199.31	304.44	–	258.64	–	–
	E_4	195.67	–	–	–	–	–
	E_{tot}	**785.88**	**919.02**	**767.25**	**772.74**	**807.67**	**908.59**
	$\overline{E}$	*196.47*	*306.34*	*383.63*	*257.58*	*403.83*	*454.29*
Ponte Cannella Vallone	E_1	217.96	268.30	310.75	321.83	352.85	391.76
	E_2	242.88	258.47	361.62	286.65	384.68	430.81
	E_3	253.74	321.83	–	350.07	–	–
	E_4	262.16	–	–	–	–	–
	E_{tot}	**976.75**	**848.60**	**672.37**	**958.55**	**737.53**	**822.57**
	$\overline{E}$	*244.19*	*282.87*	*336.19*	*319.52*	*368.76*	*411.28*

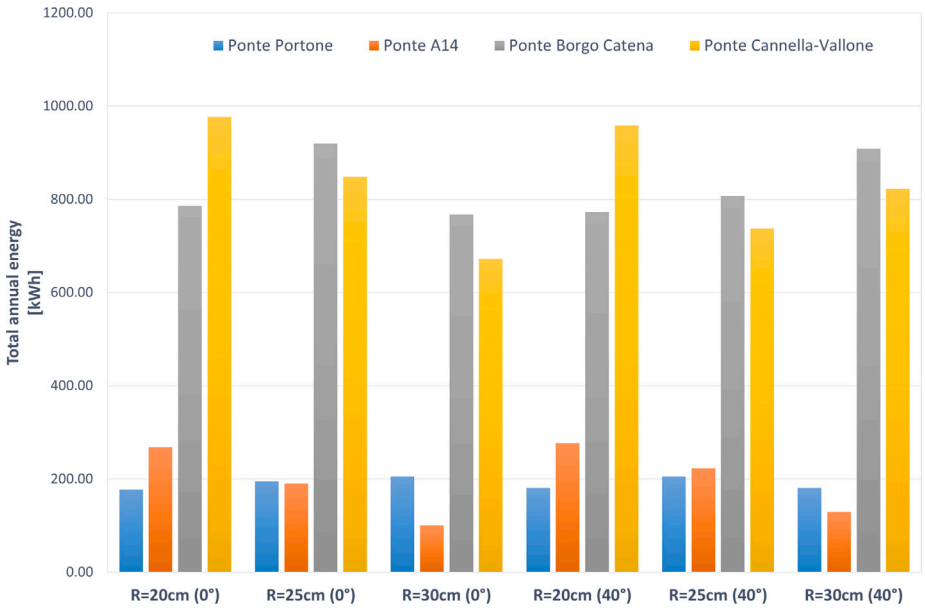

Fig. 14. Total annual energy at the selected locations and considering all tested configurations.

because the installed turbines are 2 for both $R = 25$ cm and $R = 30$ cm, in the latter case generating more power. According with the above-used procedure, passing from $R = 20$ cm to $R = 25$ cm should provide a theoretical energy increase of ~4%. This is caused by a potential increase of the energy generated by the single turbine ($\frac{E_{k,25\ \mathrm{cm}}}{E_{k,20\ \mathrm{cm}}} \sim 1.56$, as for the previous scenario) and a decrease due to the reduction of the turbines deployed in the river cross-section (from 3 to 2, providing a coefficient of 0.67). However, at the present location, each turbine with $R = 25$ cm operates for a much shorter time than those with $R = 20$ cm, i.e. ~40% instead of ~70% of the whole year. This leads to an energy produced by the $R = 25$ cm turbine that is not 1.56 times larger than that produced by the $R = 20$ cm turbine, as theoretically expected, rather a slightly larger quantity (i.e. a coefficient slightly larger than 1). This is also confirmed by the R_{max} value, which is smaller than 25 cm at the considered cross-section (Table 3). Hence, also accounting for the turbine-number reduction, an overall energy decline establishes. Conversely, the size increase from $R = 25$ cm to $R = 30$ cm and the upkeep of the same number of turbines lead to an overall energy increase, although the operating time of the larger turbines is even shorter (i.e. ~25% of the whole year).

To better illustrate the four best configurations, Fig. 15 reports both their total annual energy production (in green) and their turbine-averaged energy production (in pale blue). Depending on the chosen cross-section, the best energy production is provided by a specific solution in terms of number, size and inclination of the turbines. This leads to different values of the turbine-averaged energy production and to different installation costs. Specifically, while the first configuration is characterized by four turbines, each one harvesting a relatively small amount of energy ($\overline{E} \cong 240$ kWh), the second and third configurations are quite similar under this viewpoint, with three turbines to be installed, each one associated to an average energy $\overline{E} = (300 - 320)$ kWh. Finally, the fourth configuration is characterized by only two turbines, with the largest average energy $\overline{E} \cong 450$ kWh each.

Table 4, together with Figs. 14 and 15, shows that each single turbine of the 40° configurations harvests the highest energy, being the invested area much larger than those characterizing the 0° configurations. However, the larger is the inclination, the smaller is the number of turbines that can be installed at a specific cross-section, this leading to an overall reduction of the harvested energy.

Despite the reduced number of turbines and reduced operating time, the use of a turbine with the largest radius, even larger than the maximum radius reported in Table 3 is the optimal choice in terms of energy production per turbine (see cross-section Ponte Borgo Catena in Fig. 15), providing a total annual energy production similar to the one reached in the other cross-section with a larger number of smaller turbines. The four selected configurations depicted in Fig. 15 are sketched in Fig. 16.

Following the above considerations, the choice of the optimal configuration depends on many factors, which are only partially related to the time-varying flow discharge and the distance from the river mouth. In particular, important are the cross-section geometry and the main features of the available turbines (as depicted in Figs. 14 and 15), as well as the proximity of a bridge (due to installation reasons). Hence, the hydraulic modeling of the river at hand (including the duration curve and the activation threshold) is important to characterize the flow that can be exploited at each potentially selected cross-section, while the turbine type and geometry are fundamental to plan a suitable installation of the array of turbines. Furthermore, when installing a turbine, the activation threshold is of great importance, as it leads to longer working periods of the turbine during the year, avoiding "dead periods".

Among the turbine deployment, a floating platform might be used to host one or more submerged turbines underneath and the generator on top of the platform itself, as already discussed some years ago by some researchers [32]. More recently, the publication of specific patents shows the interest of the international community for such a topic and the feasibility of a floating platform solution to host small-sized hydrokinetic turbines to be installed along rivers [33].

Related to the installation is also the number of turbines to be deployed: the more are the turbines, the more (or larger) are the platforms to be arranged/secured along the river. This aspect is also important under the economic point of view, as the cost of the whole investment strongly depends on the chosen number of turbines.

3.4. Analysis of turbine performance

With the aim to investigate the turbine performances, some considerations can be done in terms of: (i) alternative turbine applications and (ii) evaluation of the Archimedean turbine performance.

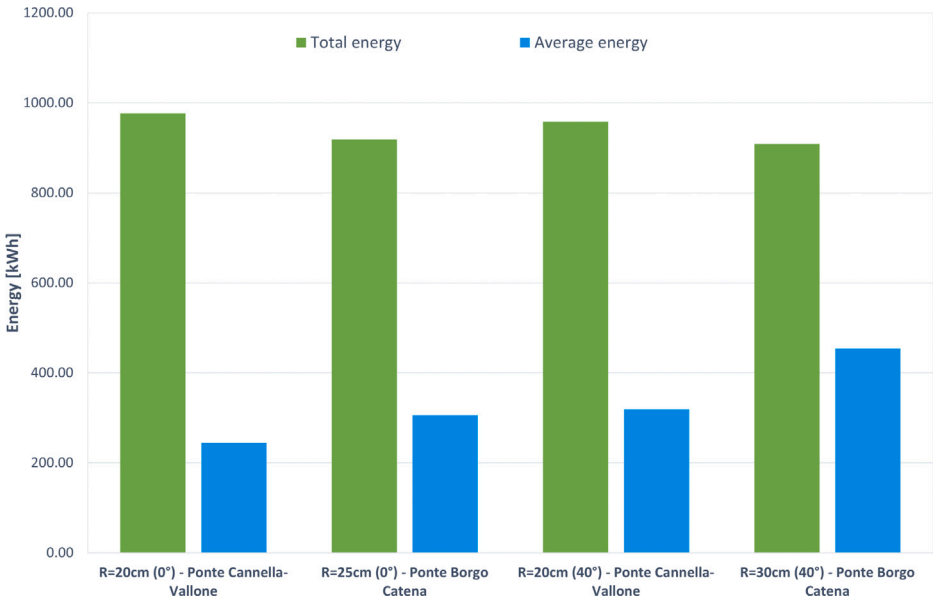

Fig. 15. Total annual energy (green bars) and average energy per turbine (pale blue bars) for the four best configurations.

3.4.1. Alternative turbine applications

The selection of potential alternatives to the studied Archimedean turbines, suggests the analysis of well-known machines like:

- a Savonius turbine (e.g., see [37]), characterized by a maximum performance coefficient $C_p = 0.2$ for $TSR = 0.8$;
- a horizontal axis propeller turbine (e.g., see [38] with a maximum $C_p = 0.37$ for $TSR = 2.5$;
- a H-Darrieus cross-flow hydrokinetic turbine (e.g., see [39]), with a maximum $C_p = 0.8$ achieved for $TSR = 2.75$.

A comparable size and the same numbers of deployed turbines are accounted for at Ponte Borgo Catena, in order to consistently compare such turbines with the analyzed Archimedean screw turbine. Using the mentioned coefficients and estimating the total annual energy, it is possible to estimate an increase, with respect to the energy estimated for the flow-aligned configuration with $R = 0.25$ m (see Fig. 15), of about 6%, 54% and 330% for the Savonius [37], the horizontal-axis [38] and the H-Darrieus [39] turbines, respectively.

However, it is worth noticing that the horizontal axis and H-Darrieus turbines operate at a rotational speed ω that is around three times larger than the optimal rotational speed of the Archimedean and Savonius turbines, and operate in a conveyance system that is not included in the other turbine installations. Hence, since such devices must preserve as much as possible the environment where they are installed, low rotation speeds are preferable, especially with the aim to avoid/minimize both harming aquatic organisms and affecting the riverbed in terms of erosion/deposition patterns [40,41]. From this perspective, Archimedes and Savonius turbines are less impactful.

3.4.2. Variability of the archimedean turbine performance

We selected two of the best configurations illustrated in Fig. 15, i.e. those located nearby Ponte Borgo Catena. The flow-aligned configuration ($\theta = 0°$) is associated with $TSR = 0.75$ and $C_p = 0.238$, which provide a total annual energy $E_{tot} = 919.02$ kWh, while the inclined configuration ($\theta = 40°$) is associated with $TSR = 1$ and $C_p = 0.313$, providing $E_{tot} = 908.59$ kWh.

The variation of the turbine performance is here evaluated starting from the variation of the cross-section-averaged velocity V, characterized by an annual time-averaged value $\overline{V} = 1.10$ m/s and a standard deviation $\sigma_V = 0.22$ m/s. Hence, a range of velocity variation is evaluated, i.e. $V_{range} = \overline{V} \pm \sigma_V = (0.8811.32)$ m/s. Then, based on the time-averaged velocity, it is possible to estimate an optimal rotation speed of the turbine

$$\omega_{opt} = (TSR_{opt} V)/R \tag{6}$$

corresponding to 3.30 rad/s and 3.67 rad/s, respectively for the flow-aligned and inclined configurations.

This allows one to estimate the TSR variation based on the range of velocity variation:

$$TSR_{range} = \frac{\omega_{opt} R}{V_{range}}, \tag{7}$$

which is $(0.62 - 0.94)$ and $(0.83 - 1.25)$ for the flow-aligned and inclined configurations, respectively. The performance coefficients referring to such ranges are then evaluated (Fig. 8), together with the annual total energy obtained using the limit values of the ranges and the potential reduction with respect to the total energy reported in Table 4 and Fig. 15.

The results are illustrated in Table 5, which shows that a significant harnessed energy reduction occurs for the inclined configurations, while a very little reduction would occur for the flow-aligned configurations, which show a better and more adaptive behavior.

4. Conclusions

The present work illustrates the importance of a detailed hydraulic modeling to properly understand what is the best option to extract energy from hydrokinetic turbines. From the analysis of the available river-stage measurements, the typical year has been obtained and used for the model validation. Field measurements have been then used at the boundaries of the analyzed river stretch, to take into account both river current and sea forcing.

The unsteady simulation carried out for the whole reference year 2018 allowed us to extract information required for the energy analysis, and to hypothesize potential turbine configurations at specific cross-sections. The different scenarios accounted for different sizes and orientations of the turbines, and consequently different numbers within each array that characterize each specific cross-section. Among the best solution, the installation should be done nearby either Ponte Cannella-Vallone (7.87 km from the MR mouth) or Ponte Borgo Catena (4.03 km from the MR mouth). At the former site, the best option is provided by four turbines with radius $R = 20$ cm, in the latter site by three turbines with $R = 25$ cm, in both cases aligned with the

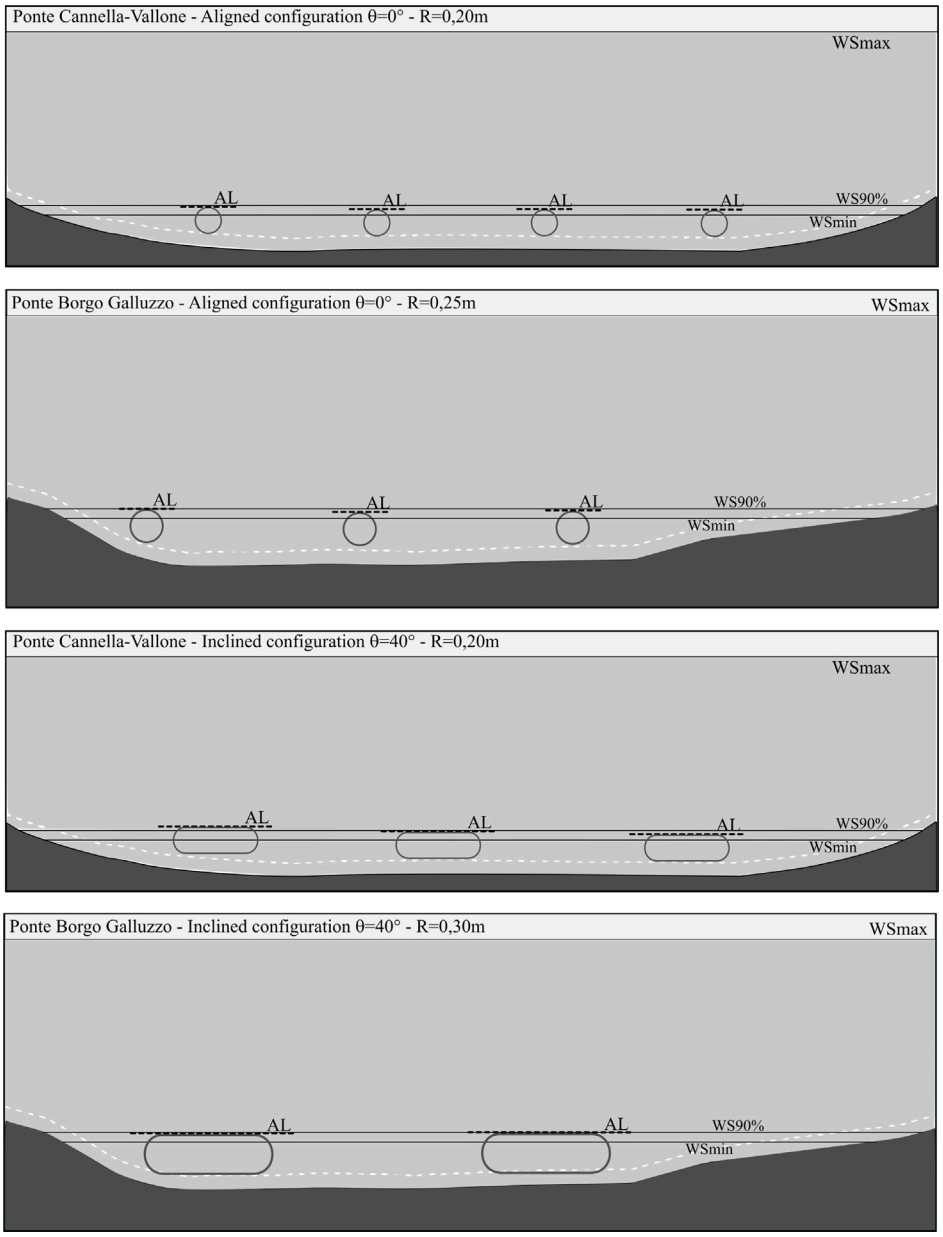

Fig. 16. Best configurations as illustrated in the total annual energy production depicted in Fig. 15.

Table 5
Analysis of annual energy reduction for the two best configurations at Ponte Borgo Catena.

Type	Flow-aligned ($\theta = 0°$)		Inclined ($\theta = 40°$)	
E_{tot} [kWh]	919.02		908.59	
TSR_{range}	0.62	0.94	0.83	1.25
$C_{p,range}$	0.231	0.224	0.305	0.236
$E_{tot,range}$ [kWh]	891.99	885.37	864.96	685.07
Annual energy reduction [%]	3	4	5	25

primary flow of the river. These and two alternative solutions, with an inclination of 40° from the streamwise direction, would lead to an annual energy production around $(0.95 - 1)$ MWh, which is in line with the consumption of community services (e.g., electricity for schools, kindergartens in small-sized urban areas [42]), as also testified by the annual electricity consumption in Italian school buildings, this being around 50 kWh/m^2 [43].

The potential uncertainty of the turbine performance coefficient may lead to an annual energy reduction up to 25% occurs for the inclined configurations, while an almost negligible reduction would occur for the flow-aligned configurations. These, thus, demonstrate a better and more adaptive behavior. In addition, the alternative use of other turbines (e.g., Savonius, horizontal-axis, H-Darrieus) may provide an increased total annual energy, though at large rotational speeds or using conveyance systems.

Under a practical viewpoint, the final deployment of the turbines is related to practical requirements, like the need of either fixed structures (usually too intrusive, leading to undesired erosion/deposition

patterns) or floating platforms, able at: (i) well adapting to the varying river stage, (ii) securing the turbine in safe way to existing structures (e.g., bridge piers or deck), (iii) hosting a generator onboard.

CRediT authorship contribution statement

Matteo Postacchini: Writing – review & editing, Writing – original draft, Supervision, Resources, Methodology, Formal analysis, Data curation, Conceptualization. **Gianluca Zitti:** Writing – review & editing, Writing – original draft, Supervision, Methodology, Data curation, Conceptualization. **Eleonora Perugini:** Writing – review & editing, Writing – original draft, Validation, Supervision, Investigation, Formal analysis, Data curation. **Riccardo Rossetti:** Writing – original draft, Methodology, Investigation, Formal analysis. **Maurizio Brocchini:** Writing – review & editing, Supervision, Investigation, Funding acquisition.

Declaration of competing interest

The authors declare the following financial interests/personal relationships which may be considered as potential competing interests: Maurizio Brocchini reports financial support was provided by Italian Ministry of University and Research. Maurizio Brocchini reports financial support was provided by US Department of Defense. Maurizio Brocchini reports was provided by Office of Naval Research Global. If there are other authors, they declare that they have no known competing financial interests or personal relationships that could have appeared to influence the work reported in this paper.

Acknowledgments

The work was partially funded under the National Recovery and Resilience Plan (NRRP), Italy, Mission 4 Component 2 Investment 1.3 - Call for tender No. 341 of 15/03/2022 of Italian Ministry of University and Research funded by the European Union – NextGenerationEU. Award number: PE00000005, Concession Decree No. 1522 of 11/10/2022 adopted by the Italian Ministry of University and Research, D43C22003030002, “Multi-Risk sciEnce for resilienT commUnities undeR a changiNg climate” (RETURN) - Cascade funding - Spoke VS1 “Acqua”, Italy, Concession Decree No. 2812 of 09/01/2024 adopted by the General Director of Politecnico di Milano, “Mitigation and Adaptation in Resilient Coastal and estUarine integrated unitS” (MARCUS). The US Department of Defense, through MINELAB SERDP Project MR23-3968 (Contract No. W912HQ23P0016), and the Office of Naval Research Global (UK), through the MORSE Project (Research Grant N62909-17-1-2148) are acknowledged.

References

[1] O. Edenhofer, R. Pichs-Madruga, Y. Sokona, K. Seyboth, P. Matschoss, S. Kadner, T. Zwickel, P. Eickemeier, G. Hansen, S. Schlömer, et al., Special report on renewable energy sources and climate change mitigation (SRREN), 2011.
[2] P.K. Yadav, A. Kumar, S. Jaiswal, A critical review of technologies for harnessing the power from flowing water using a hydrokinetic turbine to fulfill the energy need, Energy Rep. 9 (2023) 2102–2117.
[3] H.J. Vermaak, K. Kusakana, S.P. Koko, Status of micro-hydrokinetic river technology in rural applications: A review of literature, Renew. Sustain. Energy Rev. 29 (2014) 625–633.
[4] W. Ibrahim, M. Mohamed, R. Ismail, P. Leung, W. Xing, A. Shah, Hydrokinetic energy harnessing technologies: A review, Energy Rep. 7 (2021).
[5] K. Kusakana, H.J. Vermaak, Hydrokinetic power generation for rural electricity supply: Case of South Africa, Renew. Energy 55 (2013) 467–473.
[6] W. Awandu, R. Ruff, J.-U. Wiesemann, B. Lehmann, Status of micro-hydrokinetic river technology turbines application for rural electrification in Africa, Energies 15 (23) (2022) 9004.
[7] M.S. Güney, K. Kaygusuz, Hydrokinetic energy conversion systems: A technology status review, Renew. Sustain. Energy Rev. 14 (9) (2010) 2996–3004.
[8] D. Kumar, S. Sarkar, A review on the technology, performance, design optimization, reliability, techno-economics and environmental impacts of hydrokinetic energy conversion systems, Renew. Sustain. Energy Rev. 58 (2016) 796–813.
[9] B. Kirke, Hydrokinetic turbines for moderate sized rivers, Energy Sustain. Dev. 58 (2020) 182–195.
[10] B. Kirke, Towards more cost-effective river hydrokinetic turbines, Energy Sustain. Dev. 78 (2024) 101370.
[11] G. Saini, R. Saini, Clearance and blockage effects on hydrodynamic performance of hybrid hydrokinetic turbine, Sustain. Energy Technol. Assessments 57 (2023) 103210.
[12] M.M. Nunes, R.C. Mendes, T.F. Oliveira, A.C.B. Junior, An experimental study on the diffuser-enhanced propeller hydrokinetic turbines, Renew. Energy 133 (2019) 840–848.
[13] C.M. Niebuhr, M. Van Dijk, V.S. Neary, J.N. Bhagwan, A review of hydrokinetic turbines and enhancement techniques for canal installations: Technology, applicability and potential, Renew. Sustain. Energy Rev. 113 (2019) 109240.
[14] A. Stergiopoulou, V. Stergiopoulos, E. Kalkani, Experimental and theoretical research of zero head innovative horizontal axis archimedean screw turbines, Int. J. Energy Environ. 6 (5) (2015) 471.
[15] G. Dellinger, P.-A. Garambois, N. Dellinger, M. Dufresne, A. Terfous, J. Vazquez, A. Ghenaim, Computational fluid dynamics modeling for the design of Archimedes Screw Generator, Renew. Energy 118 (2018) 847–857.
[16] S. Simmons, G. Dellinger, M. Lyons, A. Terfous, A. Ghenaim, W.D. Lubitz, Effects of inclination angle on archimedes screw generator power production with constant head, J. Hydraul. Eng. 147 (3) (2021) 04021001.
[17] G. Zitti, F. Fattore, A. Brunori, B. Brunori, M. Brocchini, et al., Numerical investigation on the effects of the pitch angle on the efficiency of an archimedean-type turbine, in: Proceeding of the 13th European Wave and Tidal Energy Conference, EWTEC 2019, 2019.
[18] M. Shahsavarifard, A.H. Birjandi, E.L. Bibeau, R. Sinclaire, Performance characteristics of the energy cat 3EC42 hydrokinetic turbine, in: OCEANS 2015-Genova, IEEE, 2015, pp. 1–4.
[19] M. Bouvant, J. Betancour, L. Velásquez, A. Rubio-Clemente, E. Chica, Design optimization of an Archimedes screw turbine for hydrokinetic applications using the response surface methodology, Renew. Energy 172 (2021) 941–954.
[20] D. Zhang, P. Guo, Q. Hu, J. Li, Parametric study and multi-objective optimization of a ductless Archimedes screw hydrokinetic turbine: Experimental and numerical investigation, Energy Convers. Manage. 273 (2022) 116423.
[21] Z. Abbas, M. Waqas, S.S. Khan, R. Khatoon, S. Larkin, L. Zhao, Numerical and experimental investigation of an Archimedes screw turbine for open channel water flow application, Energy Sci. Eng. (2023).
[22] G. Zitti, F. Fattore, A. Brunori, B. Brunori, M. Brocchini, Efficiency evaluation of a ductless Archimedes turbine: Laboratory experiments and numerical simulations, Renew. Energy 146 (2020) 867–879.
[23] G.W. Brunner, HEC-RAS River Analysis System. User’s Manual. Version 6.0, Tech. Rep., US Army Corps of Engineers, Hydrologic Engineering Center, Davis, CA, 2021.
[24] L. Melito, M. Postacchini, A. Sheremet, J. Calantoni, G. Zitti, G. Darvini, P. Penna, M. Brocchini, Hydrodynamics at a microtidal inlet: Analysis of propagation of the main wave components, Estuar. Coast. Shelf Sci. 235 (2020) 106603.
[25] M. Postacchini, A.J. Manning, J. Calantoni, J.P. Smith, M. Brocchini, A storm driven turbidity maximum in a microtidal estuary, Estuar. Coast. Shelf Sci. 288 (2023) 108350.
[26] M. Postacchini, G. Darvini, E. Perugini, J. Martinelli, M. Ilari, M. Brocchini, Upriver propagation of tidal waves and mouth bar influence at a Microtidal Estuary: Observations and modeling, in: 39th IAHR World Congress 2022: From Snow to Sea, IAHR, 2022.
[27] A. Baldoni, E. Perugini, P. Penna, L. Parlagreco, M. Brocchini, A comprehensive study of the river plume in a microtidal setting, Estuar. Coast. Shelf Sci. 275 (2022) 107995.
[28] A. Valle-Levinson, Contemporary Issues in Estuarine Physics, Cambridge University Press, 2010.
[29] M. Gaiolini, N. Colombani, M. Mastrocicco, M. Postacchini, Seawater intrusion assessment along the Volturno River (Italy) via numerical modeling and spectral analysis, J. Hydrol. 626 (2023) 130289.
[30] M. Postacchini, L. Melito, A. Sheremet, J. Calantoni, G. Darvini, S. Corvaro, F. Memmola, P. Penna, M. Brocchini, Upstream propagating long-wave modes at a microtidal river mouth, Environ. Sci. Proc. 2 (1) (2020).
[31] A. Betz, The maximum of the theoretically possible exploitation of wind by means of a wind motor, Wind Eng. 37 (4) (2013) 441–446.
[32] G.T. Filho, Z.D. Souza, C.a.B.D. Rossi, R.M. Barros, F.D. Silva, Poraque hydrokinetic turbine, in: IOP Conference Series: Earth and Environmental Science, Vol. 12, 2010, p. 12094.
[33] J.-L. Achard, G. Balarac, Floating hydroelectric power plant for shallow rivers, 2019.
[34] R. Ramírez-Mendoza, L. Amoudry, P. Thorne, R. Cooke, S. McLelland, L. Jordan, S. Simmons, D. Parsons, L. Murdoch, Laboratory study on the effects of hydro kinetic turbines on hydrodynamics and sediment dynamics, Renew. Energy 129 (2018) 271–284.
[35] T. Zhang, W.H. Lam, Y. Cui, J. Jiang, C. Sun, J. Guo, Y. Ma, S. Wang, S.S. Lam, G. Hamill, Tip-bed velocity and scour depth of horizontal-axis tidal turbine with consideration of tip clearance, Energies 12 (12) (2019) 2450.

[36] F. Khaled, S. Guillou, Y. Méar, F. Hadri, Impact of the blockage ratio on the transport of sediment in the presence of a hydrokinetic turbine: Numerical modeling of the interaction sediment and turbine, Int. J. Sediment Res. 36 (6) (2021) 696–710.
[37] M.B. Salleh, N.M. Kamaruddin, Z. Mohamed-Kassim, Savonius hydrokinetic turbines for a sustainable river-based energy extraction: A review of the technology and potential applications in Malaysia, Sustain. Energy Technol. Assess. 36 (2019) 100554.
[38] J. Riglin, F. Carter III, N. Oblas, W.C. Schleicher, C. Daskiran, A. Oztekin, Experimental and numerical characterization of a full-scale portable hydrokinetic turbine prototype for river applications, Renew. Energy 99 (2016) 772–783.
[39] L. Cacciali, L. Battisti, S. Dell'Anna, G. Soraperra, Case study of a cross-flow hydrokinetic turbine in a narrow prismatic canal, Ocean Eng. 234 (2021) 109281.
[40] P.E. Schweizer, G.F. Cada, M.S. Bevelhimer, Estimation of the Risks of Collision or Strike to Freshwater Aquatic Organisms Resulting from Operation of Instream Hydrokinetic Turbines, Tech. Rep., Oak Ridge National Lab.(ORNL), Oak Ridge, TN (United States), 2010.
[41] E. Brown, S. Sulaeman, R. Quispe-Abad, N. Müller, E. Moran, Safe passage for fish: The case for in-stream turbines, Renew. Sustain. Energy Rev. 173 (2023) 113034.
[42] M. Postacchini, E. Di Giuseppe, A.L. Eusebi, L. Pelagalli, G. Darvini, G. Cipolletta, F. Fatone, Energy saving from small-sized urban contexts: Integrated application into the domestic water cycle, Renew. Energy 199 (2022) 1300–1317.
[43] A. D'Amico, D. Panno, G. Ciulla, A. Messineo, Multi-energy school system for seasonal use in the mediterranean area, Sustainability 12 (20) (2020) 8458.